RESEARCH ARTICLES

The 404 MHz wind profiler to observe precipitation

Narendra Singh[1],*, R. R. Joshi[2], S. H. Damle[2] and G. B. Pant[3]

[1]Aryabhatta Research Institute of Observational Sciences, Manora Peak, Nainital 263 129, India
[2]Indian Institute of Tropical Meteorology, Pashan, Pune 411 008, India
[3]Doon University, Motharawala Road, Kedarpur, Dehra Dun 248 001, India

This article delineates the tropical precipitation and classification of precipitating systems into stratiform and convective type, using the UHF wind profiler located at the Indian tropical station Pune (18°32′N, 73°51′E). Under moderate rain conditions the two signals arising due to clear air motions and precipitation are clearly distinguished in the power spectra. An algorithm with suitable methodology has been developed that separates clear air and precipitation echoes when they are clearly distinguishable as seen in the power spectrum. This was tested for various power spectra and found to work well under moderate rain conditions. The sensitivity of the threshold was tested for the precipitation observed on 25 July 2005. In addition, case studies of stratiform rain (precipitation observed over the site on 26 July 2005, 0800 h IST) and convective system (a thunderstorm observed on 16 May 2004) are presented and discussed. An attempt has been made to fit a Gaussian distribution curve to determine the actual Doppler shift and spectral width. The observed convective and stratiform precipitation is described in terms of reflectivity, maximum spectral width and Doppler velocity gradient in the vertical.

Keywords: Precipitation, spectral width, stratiform rain, thunderstorm, wind profiler.

TROPICAL regions generally characterized as large fields of convective clouds of all sizes, are relatively unaffected by strong baroclinic waves and fronts such as those dominating at the mid-latitudes. Therefore, the tropics present a better opportunity to assess the ensemble properties of convective clouds and precipitation. Earlier, stratiform precipitation was considered to occur primarily in the mid-latitudes in baroclinic cyclones and fronts. However, early radar observations in the tropics showed large radar echoes composed of convective rain alongside stratiform precipitation, accounting for a substantial portion of tropical rainfall[1].

Measurement of precipitation and classification of precipitating systems is an important application of meteorological radars. The vertical structure of the mesoscale convective system (MCS) has been studied extensively using ground-based and airborne Doppler weather radar. Leary and Houze[2,3] developed a conceptual model of spatial and temporal evolution of MCS. This model divides the MCS into two major cloud types, namely convective and stratiform. High temporal and spatial resolution of wind profilers made it possible to observe the precipitating systems closely, and based on extensive analysis of spectral moment data of wind profiler radars, Williams *et al.*[4] introduced mixed stratiform/convective category and subdivided the convective system into deep convective and shallow convective types.

In a deep precipitating tropical cloud system, the stratiform precipitation region is typically one of older convection[5]. It has been observed that only 10% of the rain area in a MCS is covered by convective rain showers and the remainder of the area is covered by stratiform rain[1]. The GARP Atlantic Tropical Experiment (GATE) conducted over the Atlantic in 1974 revealed that stratiform precipitation was about 40% of the tropical rainfall[6,7]. A reasonably good account of studies on precipitation can be found elsewhere[8–12].

The sensitivity of the profiler radar to Rayleigh scattering depends on its operating wavelength. Because of the high wavelength (~ 6 m) for 50 MHz systems and the inverse fourth-power dependence on wavelength of the returned power for Rayleigh scattering, sensitivity is the poorest for hydrometeor detection compared to the UHF radars with wavelengths less than 1 m. It is quantified in terms of the artificially defined equivalent reflectivity factor (Ze) as derived by Rogers *et al.*[13], which is given as

$$\mathrm{dBZe} = 10 \log \mathrm{Ze} = 10\{\log C_n^2 + \log \lambda^{11/3} + 15.13\}, \quad (1)$$

where C_n^2 (m$^{-2/3}$) is the refractive index structure variable obtained assuming the hydrometeor return as a clear air signal and λ is the radar wavelength in metres. The above equivalence is fictitious and used for convenience of analysis, since Rayleigh scattering cannot be treated as Bragg scattering. The clear air C_n^2 values over the observation site are almost always in the range 10^{-15}–10^{-17} m$^{-2/3}$, rising to values of 10^{-14} in the regions of very high turbulence (particularly at lower heights)[14], and

going down to values of 10^{-18} to 10^{-19} for weak/very weak turbulence regions at greater heights. The Z value obtained from the equivalent reflectivity factor (Ze) can be utilized to estimate true fall velocity. From the experimental findings of Joss and Waldvogel[15], in the absence of the exact knowledge of the form of the drop size spectrum, the best estimate of true fall velocity is given by $V_f = 2.65Z^{0.107}$ ms^{-1}. This gives results within ± 1 ms^{-1}, depending on the various rain rates and types of rain. Based on experimental work of Gunn and Marshall[16], Atlas et al.[17] proposed that the true fall velocity of snow is given as $\langle V \rangle_{snow} = 0.817Z^{0.063}$. Typical values of equivalent reflectivity factor (Ze) for snow, at a given C_n^2 (10^{-15}) over various operating wavelengths, are given in Table 1.

Profilers at VHF and UHF range are mainly used for clear air study, but they are also being increasingly used for precipitation studies[18]. It is thus seen that the 404 MHz wind profiler at the India Meteorological Department (IMD), Pune can be utilized for precipitation-related studies and has the capability of distinguishing between clear air and precipitation signals under normal rain rate cases, between fractions of a millimetre to a few millimetres per hour. This, of course, requires a carefully designed search algorithm for analysis of the Doppler spectra obtained by the profiler. To achieve this objective one needs to understand the typical signal-processing procedures adopted in the wind profilers. The major objective of this article is to quantify the sensitivity of a 404 MHz wind profiler to detect clear and precipitation signals simultaneously and separating them into the respective regimes in terms of Doppler velocity gradient (DVG), reflectivity and spectral width. Also, classification of the observed precipitating systems with this profiler is of importance in further studying and understanding the cloud microphysics over the site of interest. In the next section, the database is discussed followed by brief reviews of the design algorithm and associated aspects.

Database for preliminary examination

In this case study, observations taken by the Pune wind profiler during the thunderstorm activity on 10 May 2004 are presented as a case study of convective rain; observation on 25 July 2005 at 0800 h local time (IST) dataset for separating clear air echo from the precipitation signal, and 26 July 2005, 0800 h IST dataset for the case of stratiform rain. Apart from the routine observations at

Table 1. Equivalent reflectivity factor (dBZe) and fall velocity of snow for various radar frequencies at $C_n^2 = 10^{-15}$

C_n^2 (m$^{-2/3}$)	dBZe	$\langle V \rangle_{snow}$ (ms^{-1})	Radar frequency (MHz)
10^{-15}	+23	1.14	53
	–9	0.71	400
	–28	0.54	1357

0800 h IST, 1100 h IST and 14 h IST of 16 May 2004, the system was operated continuously after 15–2000 h IST, the just before the start of the rain and after one hour of the rain.

Algorithm and its components

Signal flow in a profiler system

The clear air radar echo is always very low (C_n^2 ranges between 10^{-15} and 10^{-17} m$^{-2/3}$), and the signal is almost buried well below the prevailing system noise. In case of the Pune profiler, the atmospheric clear air signal remains correlated for a sufficiently long time compared to the pulse repetition period of the profiler radar system. It is therefore possible to integrate a sufficiently large number of radar pulse returns along with noise. Since the noise samples only add incoherently, whereas the atmospheric signal returns add coherently, hence in this process, a 'n_c' pulse integration improves the power signal-to-noise ratio (SNR) by a factor of n_c. Practically, the effects of coherent integration of the complex time samples are to enhance SNR, whereas the noise power is reckoned over the total band width of the low pass filter (band width). However, it would not result in any SNR enhancement, if the noise power is limited to the same band width as that of the signal power[19]. Further spectral processing of such integrated data series can lead to improvement in the signal detectability as long as the total signal-processing duration is well within the correlation time of the atmospheric signal. If T is the pulse repetition period of the profiler radar and n_c return echoes are integrated, the unambiguous velocity measurement window of the profiler becomes $\pm \lambda/4n_cT$, where λ is the operating wavelength of the profiler. The spectral processing of M number of n_c integrated samples then provides a Doppler measurement resolution of $\Delta V = \lambda/2Mn_cT$. One thus obtains power spectral values at M points in the Doppler spectral plane spanning a velocity range of $\lambda/2n_cT$. The echo signal may lie at or around any of these M points and has to compete with the noise power present at the spectral points for being detected reliably as a signal. It is therefore necessary that one objectively estimates the average noise power density and its standard deviation in the spectrum.

Objective determination of spectral noise power

In the profiler data processing two approaches are used in the estimation of the noise level. One is the method proposed by Hildebrand and Sekhon[20] and further discussed in detail by Petitdidier et al.[21], and the other, the so-called segment method by Tsuda[22] and Sato[23]. Both the methods basically utilize the statistical properties of noise. The spectral density $P(f)$ is calculated by Fourier transforming the complex time series of radar return

Table 2. Various $|e|$ values for corresponding number of segments (K_m)

K_m	$|e|$	K_m	$|e|$	K_m	$|e|$	K_m	$|e|$
2	0.564190	11	1.586436	20	1.867475	200	2.746042
3	0.846284	12	1.629228	30	2.042761	300	2.877767
4	1.029375	13	1.667990	40	2.160777	400	2.968178
5	1.162964	14	1.703382	50	2.249074	500	3.036699
6	1.267206	15	1.735913	60	2.319278	600	3.091702
7	1.352178	16	1.765991	70	2.377359	700	3.137548
8	1.423600	17	1.793942	80	2.426774	800	3.176791
9	1.485013	18	1.820032	90	2.469700	900	3.211056
10	1.538753	19	1.844482	100	2.507594	1000	3.241436

echoes in the presence of noise, which in most cases far exceeds the atmospheric echo signal. If the amplitude distribution of noise is assumed to be Gaussian, the power spectrum distribution is typically chi-square. In the estimation of the average noise power by either of the two methods, advantage is taken of the fact that the chi-square distribution approaches a Gaussian distribution once the number of noise (power) samples used in the estimation of the average noise power is sufficiently large (> 10).

In the practical implementation of either of the two methods of noise estimation, it is desirable to take a simple three- or five-point running average of the spectral points to eliminate spiky noise contamination (interference or clutter signals) before subjecting the spectral values to further analysis. In the segment method as cited in the references 22 and 23, the value of correction factor ($|e|$) depends on the value of the number of segments (K_m) in the power spectral frame. The calculated values of $|e|$ for different values of K_m are given in Table 2. The Pune wind profiler utilizes the method of Hildebrand and Sekhon for noise estimation.

Distinction between clear air and Doppler precipitation

Once the average noise power is objectively estimated by any of the above methods, one is now ready to further classify Doppler signal spectrum in terms of clear air and precipitation (apparent fall velocity) echo. During precipitation the hydrometeors are falling through the atmosphere in the presence of clear air motions – updrafts or downdrafts. If V_{obs} is the radar observed velocity of the precipitation echo and W is the clear air velocity, then

$$V_{obs} = V_{True} - W, \tag{2}$$

where W is taken positive for updrafts of clear air motion, and thus a downdraft increases the observed hydrometeors fall velocity whereas the updraft reduces it. The value of true hydrometeor fall velocity (V_{True}) in the absence of clear air motion can be estimated from

theory[15,17,24], and is a weak function of the reflectivity factor. For the Pune profiler, the lowest detectable refractive index turbulence structure constant C_n^2 is typically about 10^{-17} m$^{-2/3}$, and this translates into a minimum detectable dBZe of –23.40 (i.e. the reflectivity factor nearly $Z = 0.006$, using the standard relation $Z = 200R^{1.6}$), which typically corresponds to a rain rate of around 1/1000 mm h^{-1} (extremely small drizzle), say for stratiform rain. Since the dynamic range of the profiler receiver system is typically in excess of 60 dB, a precipitation Doppler signal corresponding to the reflectivity factor value of almost 40 dBZe (rain rate of almost 13.5 mm h^{-1}) would also be detectable without receiver saturation. The 400 MHz wind profiler system would thus be able to faithfully reproduce the clear air and precipitation signals as long as the precipitation rate is moderate (say less than 15 mm h^{-1}). The classification search algorithm to be used in the spectral analysis of the observed datasets then needs suitable Doppler spectra limits and some other signal characteristics to enable one to complete the task. Many authors[13,25–27] have elaborated upon the classification of rain types (convective or stratiform) by study of the precipitation spectra as observed by profiler radars. The procedure followed here for identifying clear air and precipitation signals is similar to the one published by Kobayashi and Adachi[28], although our procedure has been arrived at independently. The following section enumerates various steps in this spectral analysis algorithm for classification and detection of the clear air and precipitation signals.

Threshold for signal classification

For every range bin in the spectra one gets N number of spectral (point) values, where N is the number of fast Fourier transform (FFT) points used for spectral estimation; the following operations are designed for the profiler at Pune, based on the methods discussed above.

(i) Replace the power spectral values of the central spectral point by the mean of values from two spectral points on its either side. This is done to eliminate instrumentation DC bias from the spectra.

(ii) Estimate the mean noise power (P_N) per range bin and its standard deviation (σ_N).

(iii) Subtract the mean noise power per bin from each spectral power value and obtain the array of noise power values in the spectrum distribution (bipolar) around the mean.

(iv) The next step in the algorithm would be to segregate the spectrum in different Doppler regions and initiate a search for spectral power values larger than $1.5\sigma_N$ and their corresponding Doppler bin numbers.

(v) For identifying clear air motion signal, select the portion of the spectrum corresponding to the velocity (positive downwards towards the radar-positive Doppler frequency) interval of $+1$ ms^{-1} to -6 ms^{-1}, if the range value selected is ≤ 5.25 km and identify the Doppler bin where the power spectral values are $\geq 1.5\sigma_N$. At this stage it may become necessary to further smoothen this spectral region by taking a suitable running average over the Doppler bins.

(vi) Locate the peak spectral value and its Doppler bin number amongst the identified Doppler bins. Fit a Gaussian distribution function around this peak as mean and σ_s as best fitting standard deviation. The Doppler bin corresponding to the peak then represents the average clear air velocity and $2\sigma_s$ is its spectral width. In the event of large clear air updrafts, the Doppler precipitation signal can fall in this selected Doppler span in the above procedure, particularly when the dBZe value for precipitation is very small. In that event that two peaks are likely to be identified in this selected Doppler span. Gaussian fitting or moment estimation is then required to be done for both the peaks and corresponding spectral values on either side of the peak, to estimate the mean velocities and spectral widths for both the signals. Further separation or identification could then need additional checks like range (vertical) continuity and temporal persistence of the signals.

(vii) The precipitation echo normally would lie at and beyond 1.5 ms^{-1} of the velocity scale of the spectra. The observed Doppler shift frequency would be positive. A suitable Doppler search window would therefore be (say) 1.2–10 ms^{-1}, the latter being close to the asymptotic values of fall velocity of hydrometeors or water droplets as empirically determined by Gunn and Kinzer[29] and further modified by Atlas et al.[17]. One can identify the Doppler bins where the spectral power values are $\geq 1.5\sigma_N$, and then follow the same procedure as in (vi) above to estimate the observed average fall velocity of the hydrometeors or water droplets and the spectral widths for the precipitation signal.

(viii) While differentiating clear air and precipitation signal at heights above 5.25 km (above 0°C isotherm for Pune) during the monsoon months, additional care is required because the hydrometeors at these levels may be in the form of snow or ice flakes or super-cooled water drops. Since the dielectric constant of water and snow/ice differs considerably, the latter being lower, the volume reflectivity of frozen hydrometeors at these heights is about 4.5–5 times lower than that of the water droplets of the same size/mass. The true fall velocity of these frozen hydrometeors is considerably lower and varies from 0.5 ms^{-1} to just over 1 ms^{-1}. The clear air updrafts, if any, at these heights then push them further closer to the domain of clear air velocities. As a simple method of knowing whether the hydrometeors above the 0° isotherm are super-cooled water drops or ice/snow, is to look for the absence or presence of melting layer signature just below the level of the 0° isotherm. This can be diagnosed by inspecting whether sudden, large Doppler velocity gradients exist at these heights. This would then lead to correct estimation of Ze values for heights above the melting layer. The presence of melting layer can also be diagnosed quite clearly by the sharp increase in dBZe over a narrow layer just below the 0° isotherms. However, clear air downdrafts at these heights push these precipitation signals further away from the domain of clear air velocities. It is therefore necessary to identify all the signals with spectral power values $\geq 1.5\sigma_N$ in the Doppler velocity band of -6 ms^{-1} to $+2$ ms^{-1}. An estimate of zeroeth, first and second moments, corresponding to all peak signals, identified by the procedure as described above can be subsequently computed. The final classification of the signal as clear air or precipitation would thus require additional thresholding checks and signal characteristics such as spectral width and height continuity. The observed spectral width of precipitation is expected to be larger than that for clear air signal and can be used as a test for classification.

Discussion and conclusion

Separation of clear air and precipitation signal

A first-cut software code has been developed for the algorithm as described above and sample results for 1 h
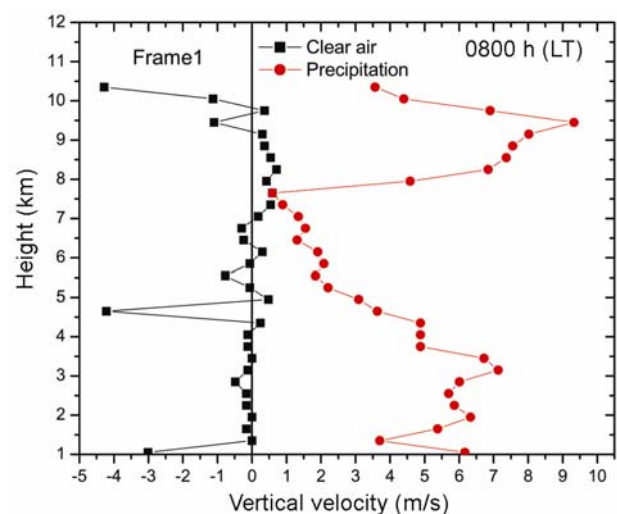

Figure 1. Observed typical clear air and precipitation signal measured in ms^{-1} (+ve downward, radar convention), 25 July 2005, 0800 h IST. This frame is a representative of the observation.
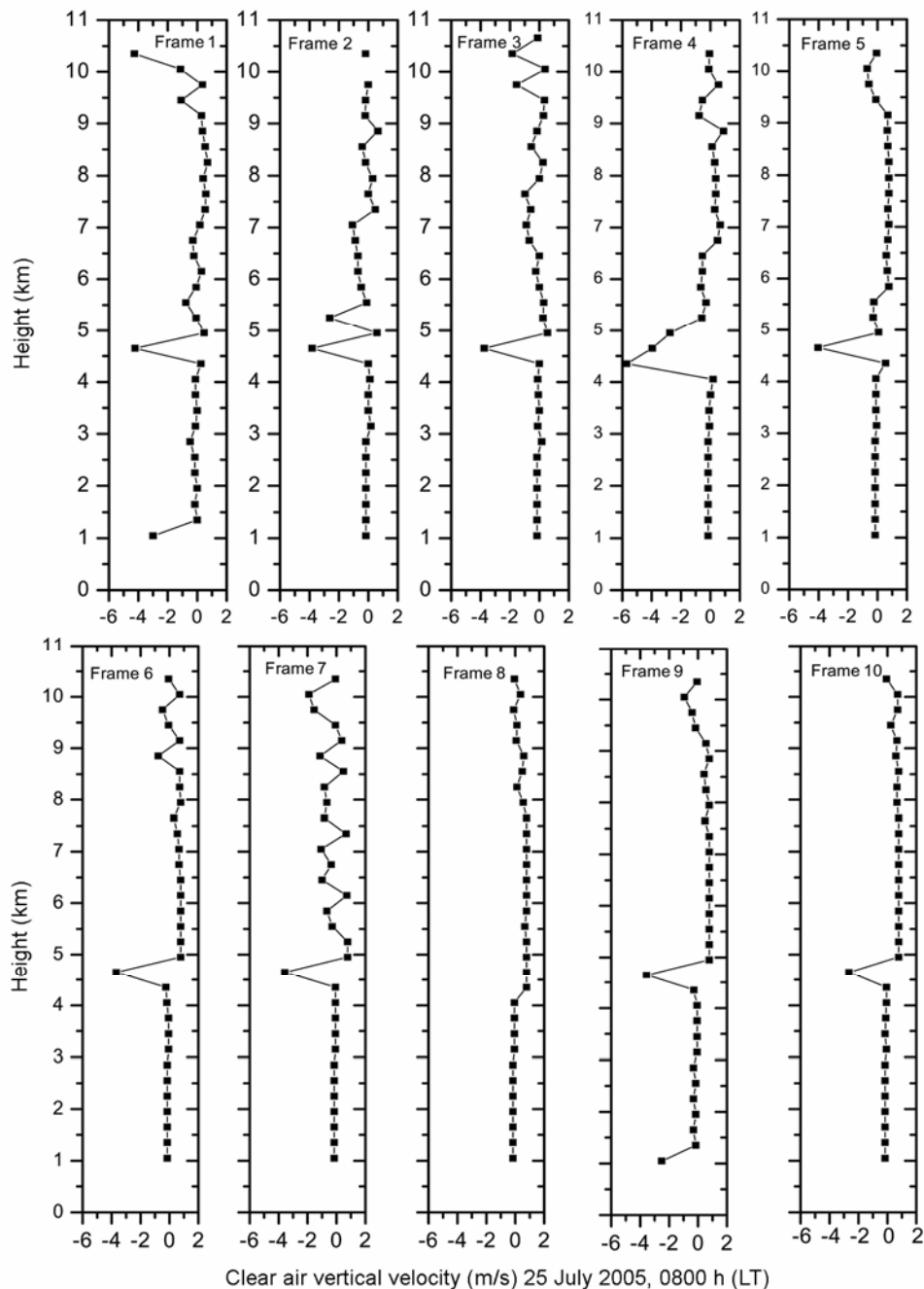
Figure 2. Clear air signal (ms^{-1}) after separation, obtained after one hour of observation on 25 July 2005, 0800 h IST.

of observations on 25 July 2005 are given in Figures 1–3. A total of 10 frames of spectra obtained in an hour were analysed for a particular range bin at 1.65 km. Figure 1 is the representative of 10 frames containing clear air as well as precipitation signals before separation, as described earlier. Figure 2 gives the separated clear air signals for all the 10 frames of the spectrum during 1 h of observation, whereas the separated precipitation echoes are shown in Figure 3.

For the range bin of 1.65 km, the clear air and precipitation echoes are shown in Figure 4 as example where Gaussian fitting of the spectra is attempted. It can be clearly seen from Figure 4 that the clear air signal power

is less by one order of magnitude compared to the power level in the precipitation spectrum. The Gaussian function fitted to the clear air and precipitation echoes is given as:

$$y = y_0 + \frac{A}{w \cdot \sqrt{\pi/2}} \exp\left(-\frac{2(x - x_0)^2}{w^2}\right), \qquad (3)$$

where y_0 is the Baseline offset, A the total area under the curve, x_0 the centre of the peak, $w = 2\sigma$ is approximately 0.849 the width of the peak at half height, $w/2$ the standard deviation and the centre (x_0) represents the mean.
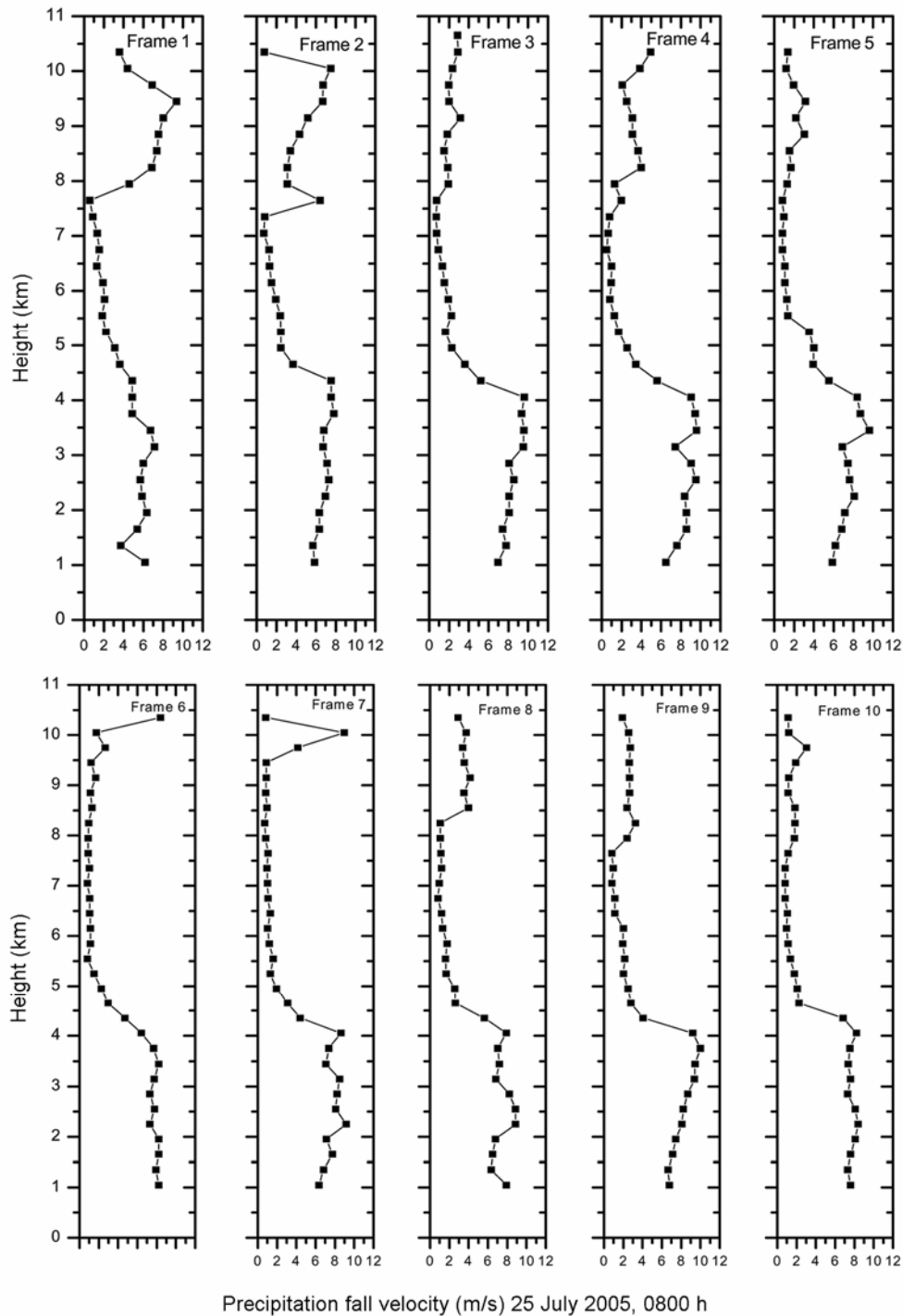
Figure 3. Precipitation signal (ms⁻¹) after separation, obtained after one hour of observation on 25 July 2005, 0800 h IST.

This model describes a bell-shaped curve like the normal Gaussian probability distribution function. The fitting parameters are given in Figure 4.

Stratiform rain

The case of stratiform rain observed on 26 July 2005 at 0800 h IST, was analysed in this study. Precipitating clouds having melting layer signature which is determined by maximum DVG between the altitudes 3.5 and 6 km, including the 0° isotherm level are characterized to be stratiform rain[4]. Figure 5 *a* shows the vertical fall velocity. An abrupt change in the fall velocity between 6 and 4 km is observed, which increases to a maximum of 8 ms⁻¹ with decreasing height in this region. Maximum velocity gradient is seen in the height region 4.05–4.65 km (marked by arrow), which implies that the solid

hydrometeors cross the 0° isotherm level and start melting, because in this region the change of phase (solid to liquid) takes place. The enhancement in SNR (Figure 5 b) between 6 and 4 km, arises due to the considerably different reflectivities of solid hydrometeors and the liquid water droplets. The volume reflectivity of the water is 4–5 times greater than that of the frozen hydrometeors and results in a strong back-scattered signal. The observed SNR in this region is in excess of 30 dB. The enhancement in the SNR is caused by various mechanisms, such as the change in the dielectric constant through melting or due to gradient (Fresnel) reflection from a layer of phase transition, change in fall velocity throughout melting, precipitation growth, aggregation and break-up among the water droplets and hydrometeors, the combined effect on echo power (of the shape and orientation of the hydrometeors) and the effect of distribution of water within the melting snowflakes (known as density effect)[30]. Corresponding equivalent reflectivity (Figure 5 c), in this region results from the breadth of drop size distribution

(DSD) as the frozen hydrometeors melt and turn into rain with the different size drops falling at different velocities. The observed equivalent reflectivity of about 5 km is as much as 20 dB in the radar resolution volume. This is the typical case of stratiform rain, as convective systems do not have the melting layer signature as explained above.
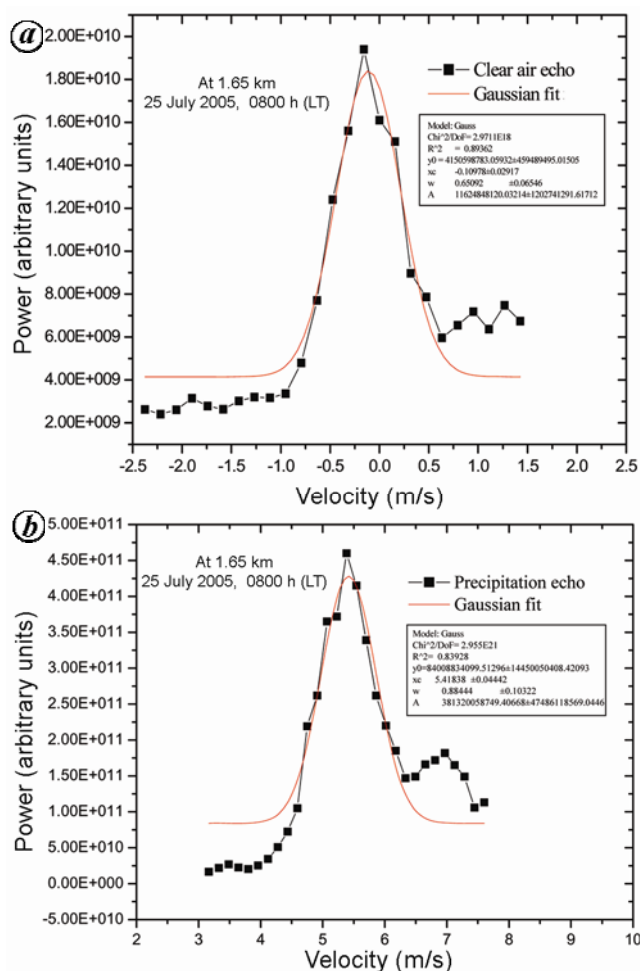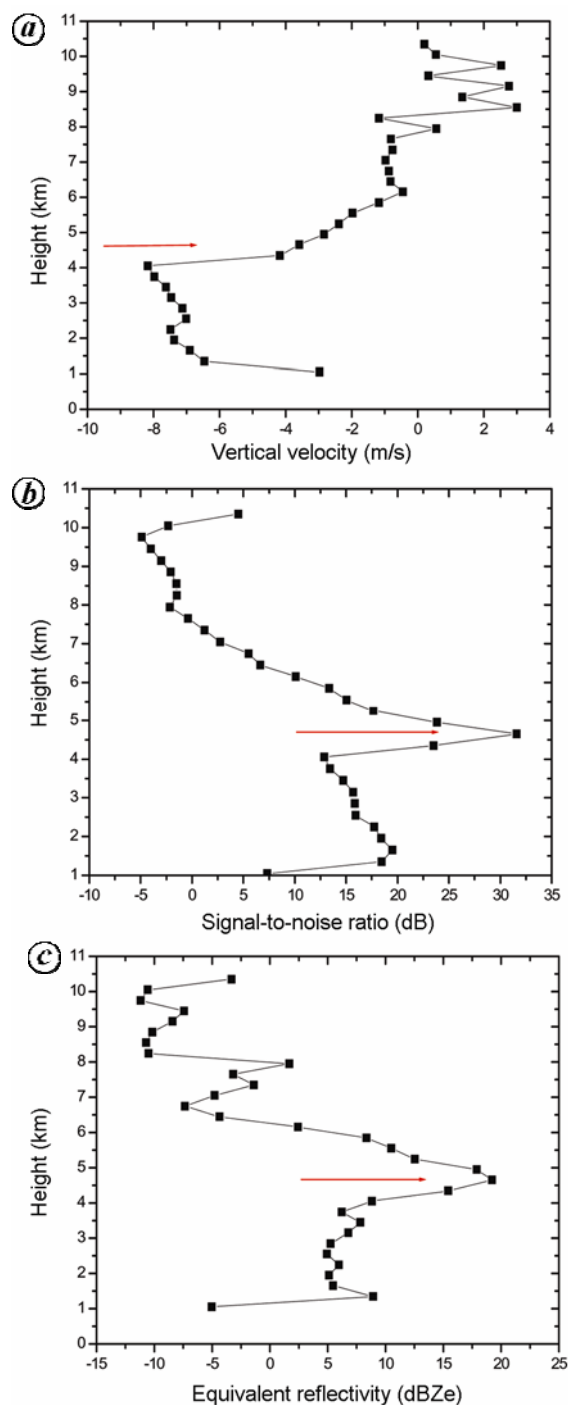

Figure 5. Altitude profile of (*a*) vertical Doppler velocity (–ve downward, met convention), (*b*) detectability signal-to-noise ratio and (*c*) equivalent reflectivity during stratiform rain, observed on 25 July 2005, 0800 h IST.

Figure 4. Gaussian fit to (*a*) clear air spectrum and (*b*) precipitation spectrum, along with the fitting parameters.

The data represented in Figure 5 *a* are actually observed fall velocity, which includes clear air signal as well. This exercise is of paramount importance in precipitation studies, and will help in a detailed understanding of the systems observed by the profiler for longer periods of observation. However, future work needs to be done to study the precipitating systems extensively over this tropical station.

Convective rain

The case study of convective rain is based on the occurrence of a thunderstorm on 16 May 2004 over the site, and is characterized in terms of patterns of vertical air motion, reflectivity and spectral width/variance (Figure 6). The UHF wind profiler is more sensitive to Rayleigh than Bragg scattering, and it actually measures the fall velocity of the hydrometeors during precipitation. Here, we have observed both the scattering regimes in the developing and decaying stages of the thunderstorm. In Figure 6 (top panel), consistent upward motions (positive vertical velocity, shaded area) of 0.5 ms^{-1} are observed from the morning (at 0800 h IST and 1100 h IST) till afternoon (1400 h IST and 1700 h IST), right from near surface to 3–4 km, and the clear air conditions prevailed during these hours of the day. These convective updrafts help in lifting sufficient amount of moisture into the upper levels of the atmosphere, to initiate the thunderstorm. However, vertical motions are observed in the upper region of the atmosphere between 5.5 and 8 km, at 1100 h IST. As the time advances, the thunderstorm gets initiated and downdrafts with vertical velocities between –1 and –4 ms^{-1} are seen in the height region of 3–8 km. In the mature stage, around 1800 h IST, the downdrafts are seen to be prevalent right from the lowest observable height of 1.05 km. Soon after this stage it starts raining and the vertical fall velocities reach values of as much as –7 ms^{-1}; however, the thunderstorm is not as strong as usual.

Figure 6 (middle panel) shows the reflectivity profile, during clear air conditions under convective updrafts. The observed reflectivity values are predominantly negative (at 0800 h IST and 1100 h IST). The reflectivity values turn positive in the afternoon (at 1400 h IST), at times touching around 20 dB once the precipitation starts falling during that period (at 1700 h IST, 1800 h IST, 1900 h IST and 20 h IST). This clearly shows the transition from the Bragg regime to Rayleigh scattering and the precipitation signals (Rayleigh scattering) dominate the UHF clear air signals during the thunderstorm (rain) period.

The velocity variance (σ^2) is a measure of the broadness of the Doppler spectral peak and represents the turbulence within the resolution volume. Figure 6 (bottom panel) shows a turbulent region with high (σ^2) values (6–8 m^2 s^{-2}) below 5 km in the thunderstorm period. This is the time (1800–1900 h IST) when heavy rain is observed over the site.

The wind profiler offers the unique ability to directly measure vertical motion profiles through precipitating and non-precipitating systems. It can detect stratiform as well as convective rain. Under moderate rain conditions Bragg and Rayleigh scattering can be identified simultaneously and in this case, separating the two signals becomes rather easy. For the case under study, the precipitation return (Rayleigh scattering) dominates the UHF signal during the thunderstorm period. A turbulent region is seen right from 1.05 to 8 km in the vertical during the thunderstorm. High reflectivity and detectability of SNR (single-pulse SNR becomes detectable after multiplying by the spectral processing gain), is observed in the height range 4.05–5 km during stratiform rain.

Most of the studies regarding precipitation with UHF wind profilers are confined to mid-and-high latitudes; very few are reported in the tropics. Hence the 404.37 MHz, profiler at IMD, is utilized for a few case studies of tropical precipitation. This preliminary study shows that the profiler has the potential for detailed study
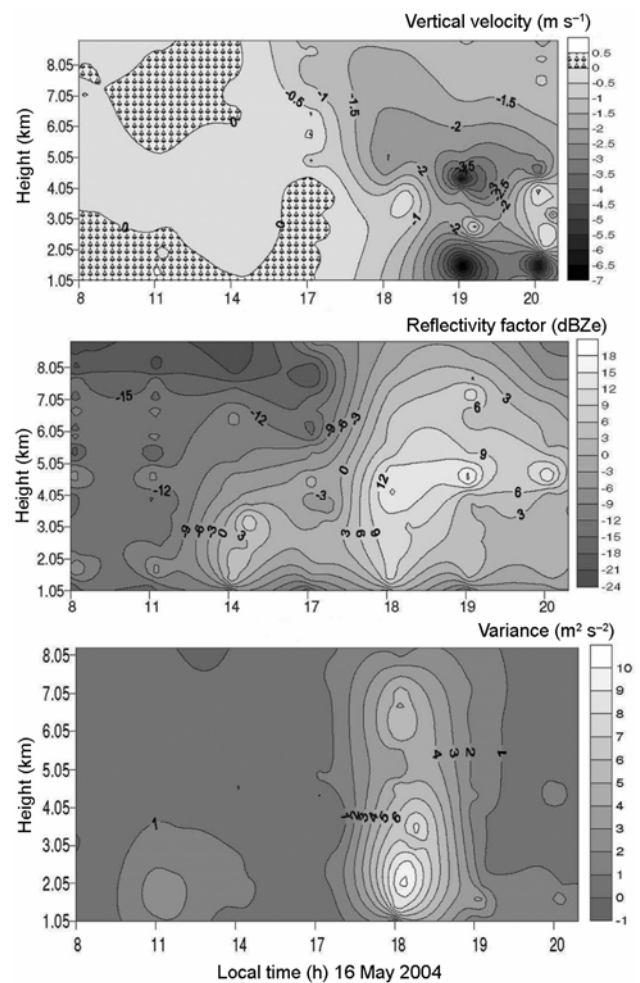

Figure 6. The observed parameters during convective rain are vertical velocity in ms^{-1}; negative values indicate downward motion (top panel), reflectivity in dBZe (middle panel) and spectral width (ms^{-1}; bottom panel).

of precipitation and thunderstorm over Pune. First-cut algorithm as presented here can be further refined for obtaining the derived products such as DSD in precipitating systems and the study of the evolution of DSD as the precipitation shifts from convective to stratiform mode. Once the other surface instruments like the sensitive disdrometer are co-located at the profiler site it would be possible to obtain quantitative estimates leading to reflectivity–rain rate (Z–R) relationships and overall understanding of the microphysics of precipitating systems through studies on the evaluation of DSD and its variation with height.

1. Houze, R. A., *Cloud Dynamics*, Academic Press, San Diego, California, 1993.
2. Leary, C. A. and Houze Jr, R. A., The structure and evaluation of convection in a tropical cloud cluster. *J. Atmos. Sci.*, 1979, **36**, 437–457.
3. Leary, C. A. and Houze Jr, R. A., Melting and evaporation of hydrometeors in precipitation from the anvil clouds of deep tropical convection. *J. Atmos. Sci.*, 1979, **36**, 669–679.
4. Williams, C. R., Ecklund, W. L. and Gage, K. S., Classification of precipitation clouds in the tropics using 915 MHz wind profilers. *J. Atmos. Ocean. Technol.*, 1995, **12**, 996–1012.
5. Houze, R. A., Stratiform precipitation in regions of convection: a meteorological paradox. *Bull. Am. Meteorol. Soc.*, 1997, **78**, 2179–2196.
6. Cheng, C. D. and Houze Jr, R. A., The distribution of convective and mesoscale precipitation in GATE radar echo pattern. *Mon. Weather Rev.*, 1979, **107**, 1370–1381.
7. Leary, C. A., Precipitation structures of the cloud clusters in a tropical easterly waves. *Mon. Wea. Rev.*, 1984, **112**, 313–325.
8. Rogers, R. R., An extension of the *Z–R* relationship for Doppler radar. In Paper presented at the 11th Weather Radar Conference. Boston, Mass., Boulder Colo, 14–18 September 1964.
9. Seliga, T. A. and Bringi, V. N., Potential use of radar differential reflectivity measurements at orthogonal polarizations for measuring precipitation. *J. Appl. Meteorol.*, 1976, **15**, 69–76.
10. Houze Jr, R. A., Observed structure of mesoscale convective systems and implications for large scale heating. *Q. J. R. Meteorol. Soc.*, 1989, **115**, 425–461.
11. Balakrishnan, N. and Zrnić, D. S., Use of polarization to characterize precipitation and discriminate large hail. *J. Atmos. Sci.*, 1990, **47**, 1525–1540.
12. Rao, T. N., Rao, D. N., Mohan, K. and Raghavan, S., Classification of tropical precipitating systems and associated Z–R relationships. *J. Geophys. Res*, 2001, **106**, 17699–17711.
13. Rogers, R. R., Ecklund, W. L., Carter, D. A., Gage, K. S. and Ethier, S. A., Research Applications of a boundary-layer wind profiler. *Bull. Am. Meteorol. Soc.*, 1993, **74**, 567–580.
14. Singh, Narendra, Joshi, R. R., Chun, H. Y., Pant, G. B., Damle, S. H. and Vashishtha, R. D., Seasonal, annual and inter-annual features of turbulence parameters over the tropical station Pune (18°32′N, 73°51′E) observed with UHF wind profiler. *Annu. Geophys.*, 2008, **26**, 3677–3692.
15. Joss, J. and Waldvogel, A., Raindrop size distributions and Doppler velocities. Preprints 14th Conference on Radar Meteorology, Tucson, AZ. *Amer. Meteorol. Soc.*, 1970, pp. 153–156.
16. Gunn, K. L. S. and Marshall, J. S., The distribution with size of aggregate snowflakes. *J. Meteorol.*, 1958, **15**, 452–461.
17. Atlas, D., Srivastava, R. C. and Sekhon, R. S., Doppler radar characteristics of precipitation at vertical incidence. *Rev. Geophys. Space Phys.*, 1973, **11**, 1–35.
18. Currier, P. E., Avery, S. K., Balsley, B. B., Gage, K. S. and Ecklund, W. L., Combined use of 50 MHz and 915 MHz wind profilers in the estimation of raindrop size distributions. *Geophys. Res. Lett.*, 1992, **19**, 1017–1020.
19. Farley, D. T., On-line data processing techniques for MST radars. *Radio Sci.*, 1985, **20**, 1177–1184.
20. Hildebrand, P. H. and Sekhon, R. H., Objective determination of the noise level in Doppler spectra. *J. Appl. Meteorol.*, 1974, **13**, 808–811.
21. Petitdidier, M., Garrouste, A. and Delcourt, J., Statistical characteristics of the noise power spectral density in UHF and VHF wind profiles. *Radio Sci.*, 1997, **32**, 1229–1247.
22. Tsuda, T., Data acquisition and processing. *Handbook for MAP*, SCOSTEP Secretariat, University of Illinois, Urbana, 1989, vol. 30, pp. 151–184.
23. Sato, T., Radar principles. *Handbook for MAP*, SCOSTEP Secretariat, University of Illinois, Urbana, 1989, vol. 30, pp. 19–53.
24. Rogers, R. R., Baumgardner, D., Ethier, S. A., Carter, D. A. and Ecklund, W. L., Comparison of raindrop size distributions measured by radar wind profiler and by airplanes. *J. Appl. Meteorol.*, 1993, **32**, 694–699.
25. Ralph, F. M., Using radar-measured radial vertical velocities to distinguish precipitation scattering from clear-air scattering. *J. Atmos. Ocean. Technol.*, 1995, **12**, 257–267.
26. Atlas, D. W., Ulbrich, C. W., Marks Jr, F. D., Amitai, E. and Williams, C. R., Systematic variation of drop size and radar-rainfall relations. *J. Geophys. Res.*, 1999, **104**, 6155–6169.
27. Rao, T. N., Rao, D. N. and Raghavan, S., Tropical precipitating systems observed with Indian MST Radar. *Radio Sci.*, 1999, **34**, 1125–1139.
28. Kobayashi, T. and Adachi, A., Retrieval of arbitrarily shaped raindrop size distributions from wind profiler measurements. *J. Atmos. Ocean. Technol.*, 2005, **22**, 433–442.
29. Gunn, R. and Kinzer, G. D., The terminal velocity of fall for water droplets in stagnant air. *J. Meteorol.*, 1949, **6**, 243–248.
30. Fabry, F. and Zawazdki, I., Long-term radar observations of the melting layer of precipitation and their interpretation. *J. Atmos. Sci.*, 1995, **52**, 838–851.